

On the α -attractor T-models

Gabriel Germán^a

^aInstituto de Ciencias Físicas, Universidad Nacional Autónoma de México, Av. Universidad s/n, Cuernavaca, Morelos 62210, Mexico

E-mail: gabriel@icf.unam.mx

Abstract. We carry out a fully analytical study of the phenomenology of α -attractor T-models defined by the potential $V = V_0 \tanh^p(\lambda\phi/M_{pl})$. We obtain expressions for the number of e-folds during inflation N_{ke} in terms of the scalar spectral index n_s and independently in terms of the tensor-to-scalar ratio r . From these expressions we obtain exact solutions for both n_s and r in terms of N_{ke} along with their expansions for large N_{ke} , in full agreement with known expressions. Eliminating the parameter λ from the model in terms of n_s and r we can obtain exact solutions for r in terms of n_s and N_{ke} which allows us to reproduce, in particular, numerical solutions presented by the Planck Collaboration for the monomial potentials. We explicitly show how these solutions are contained in the solutions for the α -attractors and are also the end points of these. Finally, by also eliminating the global scale V_0 in terms of the observables n_s and r we show how in the appropriate limit the α -attractor potential exactly reduces to the monomials potential. We also briefly show that for α -attractor E-models, which generalize the Starobinsky potential in the Einstein frame, a similar transition occurs.

Contents

1	Introduction	1
2	The α-attractor T-models	2
2.1	Slow-roll interruptus	4
2.2	The case $\lambda \geq \lambda_l$	5
2.3	The case $\lambda < \lambda_l$	7
3	Removing the λ and V_0 parameters	8
3.1	General solutions for $r(n_s, N_{ke}, p)$	9
3.2	Monomials as particular cases of α -attractors	13
4	Conclusions	15

1 Introduction

In recent years alpha attractor-type models have captivated considerable attention mainly due to the fact that they have a fairly well-understood origin in conformal and super-conformal field theories as well as their close relationship with supergravity theories [1]-[15], the fact that they connect with well known monomial potentials and most importantly, because they have a phenomenology [6] that is fully consistent with reported results by e.g., the Planck Collaboration [16]. Important properties of α -attractors have been extensively discussed in the literature (for a sample of articles in the subject see e.g., [17]-[33] and references therein). The resulting class of potentials generalized from the simplest monomials is of the form

$$V = V_0 \tanh^p \left(\lambda \frac{\phi}{M_{pl}} \right), \quad (T - models) \quad (1.1)$$

and

$$V = V_0 \left(1 - e^{-\lambda \sqrt{\frac{2}{3}} \frac{\phi}{M_{pl}}} \right)^p. \quad (E - models) \quad (1.2)$$

Connecting with the original notation $\lambda = 1/\sqrt{6\alpha}$ for T-models or $\lambda = 1/\sqrt{\alpha}$ for E-models thus, “ α ”-attractors. These potentials can be considered on its own as phenomenological potentials for inflation and as such have also been studied, mainly numerically. The main purpose of this work is to provide a fully *analytical* treatment, which can be considered as complementary to phenomenological results briefly presented in the literature [6], of the most important properties of the T-type α -attractors defined by the potential (1.1).

The organization of the article is as follows: In Section 2 we discuss in detail the end of slow-roll either with the condition $\eta = -1$ or with $\epsilon = 1$ where η and ϵ are the usual slow-roll parameters given by [34]

$$\epsilon \equiv \frac{M_{pl}^2}{2} \left(\frac{V'}{V} \right)^2, \quad \eta \equiv M_{pl}^2 \frac{V''}{V}, \quad (1.3)$$

M_{pl} is the reduced Planck mass $M_{pl} = 2.44 \times 10^{18}$ GeV which we set equal to 1 in most of what follows and primes on V denote derivatives with respect to the inflaton field ϕ . We

provide expressions for the number of e-folds N_{ke} from the time scales left the horizon at wavenumber mode k corresponding to ϕ_k to end of inflation at ϕ_e . The expression for N_{ke} when $\phi_k = \phi_k(n_s)$ is exclusively dependent on the spectral index n_s , the model characterized by p and the λ parameter appearing in the potential. This is done by obtaining ϕ_k from the equation [34]

$$n_s = 1 + 2\eta - 6\epsilon, \quad (1.4)$$

written in the form $\delta_{n_s} + 2\eta - 6\epsilon = 0$, where δ_{n_s} is defined as $\delta_{n_s} \equiv 1 - n_s$. When $\phi_k = \phi_k(r)$ we obtain the number of e-folds during inflation N_{ke} exclusively dependent on the tensor-to-scalar ratio r , p and λ by solving for ϕ_k from the equation

$$n_t = -2\epsilon = -\frac{r}{8}, \quad (1.5)$$

written in the form $r = 16\epsilon$. In this way we can obtain exact solutions for $n_s(N_{ke}, \lambda, p)$ and for $r(N_{ke}, \lambda, p)$ as well as their asymptotic behavior in various situations, mainly for large number of e-folds N_{ke} . In Section 3 we also obtain an expression for N_{ke} but this time in terms of r , n_s and p by eliminating the parameter λ in terms of n_s and r . In this case we can write any quantity of interest exclusively in terms of the observables n_s and r , the quantities so written will keep tightening as more precise determination of the observables is achieved.

Using the allowed range of λ we can deduce the range for r . In particular we find solutions for $r(n_s, N_{ke}, p)$ that allow us to study the n_s - r plane for various values of N_{ke} and p . Using an approximation for r in the large N_{ke} limit we find bounds for N_{ke} as well as a lower bound for the parameter p . We explicitly show how the predictions for $r(n_s, p)$ of the monomials potential $V_{mon} = \frac{1}{2}m^{4-p}\phi^p$ are exactly contained in the solutions for r of the α -attractor models and should also be the ending points of the curves $r(n_s, N_{ke}, p)$ [6]. To fully clarify this phenomenon we also determine the global scale V_0 in terms of n_s and r through the equation

$$A_s(k) = \frac{1}{24\pi^2} \frac{V}{M^4\epsilon}. \quad (1.6)$$

Thus, a direct study of the potential (1.1) with V_0 and λ eliminated in terms of n_s and r shows how it transitions exactly to the monomials potential in the limiting case in which the relationship between the observables r and n_s of the monomials is fulfilled and we illustrate graphically this phenomenon in Fig. 11. We show briefly that this is also the case for the type of E-models (1.2) that can be considered as generalizations of the Starobinsky model in the Einstein frame (see Fig. 12). Finally, Section 4 contains our conclusions on the main points discussed in the article.

2 The α -attractor T-models

The α -attractor T-models generalized from the simplest monomials are defined by the potential given by Eq. (1.1), where p is a positive number which distinguishes among the models and λ is a parameter. When necessary we can understand ϕ in Eq. (1.1) as its absolute value to guarantee a bounded potential from below. We do not write it explicitly anywhere because we will be working in the positive region of ϕ always unless stated otherwise. An expression for ϕ_k , the inflaton at horizon crossing, is obtained by solving Eq. (1.4), $\delta_{n_s} + 2\eta - 6\epsilon = 0$, with the result

$$\cosh^2 \left(\lambda \frac{\phi_k}{M_{pl}} \right) = \frac{1}{2\delta_{n_s}} \left(\delta_{n_s} + 4p\lambda^2 + \sqrt{\delta_{n_s}^2 + 4p^2\lambda^2\delta_{n_s} + 16p^2\lambda^4} \right), \quad (2.1)$$

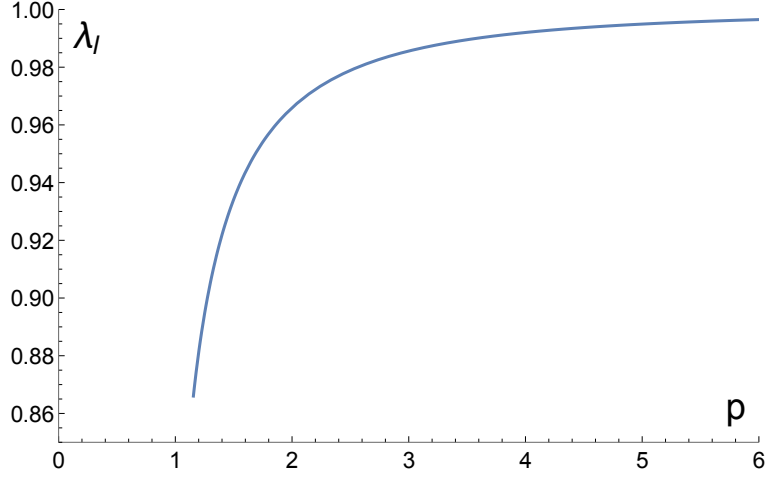


Figure 1: The figure shows the limiting value of λ as a function of p , given by Eq. (2.4), which separates solutions where the end of slow-roll is given by the condition $\eta = -1$ from those where inflation is terminated by $\epsilon = 1$. For $p = 2$, $\lambda_l \approx 0.9659$.

where δ_{n_s} is defined as $\delta_{n_s} \equiv 1 - n_s$. For large λ the end of slow-roll is given by the solution to the equation $\eta = -1$ while for small λ by the condition $\epsilon = 1$. The value of ϕ which solves the condition $\eta = -1$ is $\phi_{e\eta}$ and it is given by

$$\cosh^2 \left(\lambda \frac{\phi_{e\eta}}{M_{pl}} \right) = \frac{1}{2} \left(1 + 2p\lambda^2 + \sqrt{1 + 4p^2\lambda^2(\lambda^2 - 1)} \right), \quad (2.2)$$

while the solution for the $\epsilon = 1$ case is

$$\cosh^2 \left(\lambda \frac{\phi_{e\epsilon}}{M_{pl}} \right) = \frac{1}{2} \left(1 + \sqrt{1 + 2p^2\lambda^2} \right). \quad (2.3)$$

The solution Eq. (2.2) makes sense for $1 + 4p^2\lambda^2(\lambda^2 - 1) \geq 0$. Thus, the value of λ which separates one ϕ_e -solution from the other is obtained by solving $1 + 4p^2\lambda^2(\lambda^2 - 1) = 0$ with the result (see Fig. 1)

$$\lambda_l = \frac{1}{\sqrt{2}} \sqrt{1 + (p^2 - 1)^{1/2}/p}, \quad (2.4)$$

whenever $p \geq 2/\sqrt{3}$. The value of λ_l signals the minimum value λ can have (for a given p) when $-\eta = 1$ (see Fig. 2, in particular panel number 3). Thus, for $\lambda < \lambda_l$ the end of inflation is dictated by the condition $\epsilon = 1$ while the case $\lambda \geq \lambda_l$ requires solving the equation $-\eta = 1$ for the end of slow-roll with the solution given above. For $p = 2$, $\lambda_l \approx 0.9659$.

The number of e-folds from the time scales the order of the pivot scale left the horizon during inflation at a_k to the end of inflation at a_e is given by

$$N_{ke} = -\frac{1}{M_{pl}^2} \int_{\phi_k}^{\phi_e} \frac{V}{V'} d\phi = \frac{1}{2p\lambda^2} \left(\cosh^2 \left(\lambda \frac{\phi_k}{M_{pl}} \right) - \cosh^2 \left(\lambda \frac{\phi_e}{M_{pl}} \right) \right). \quad (2.5)$$

We can write N_{ke} in the form $N_{ke} = N_k - N_e$ where

$$N_k \equiv \frac{1}{2p\lambda^2} \cosh^2 \left(\lambda \frac{\phi_k}{M_{pl}} \right), \quad (2.6)$$

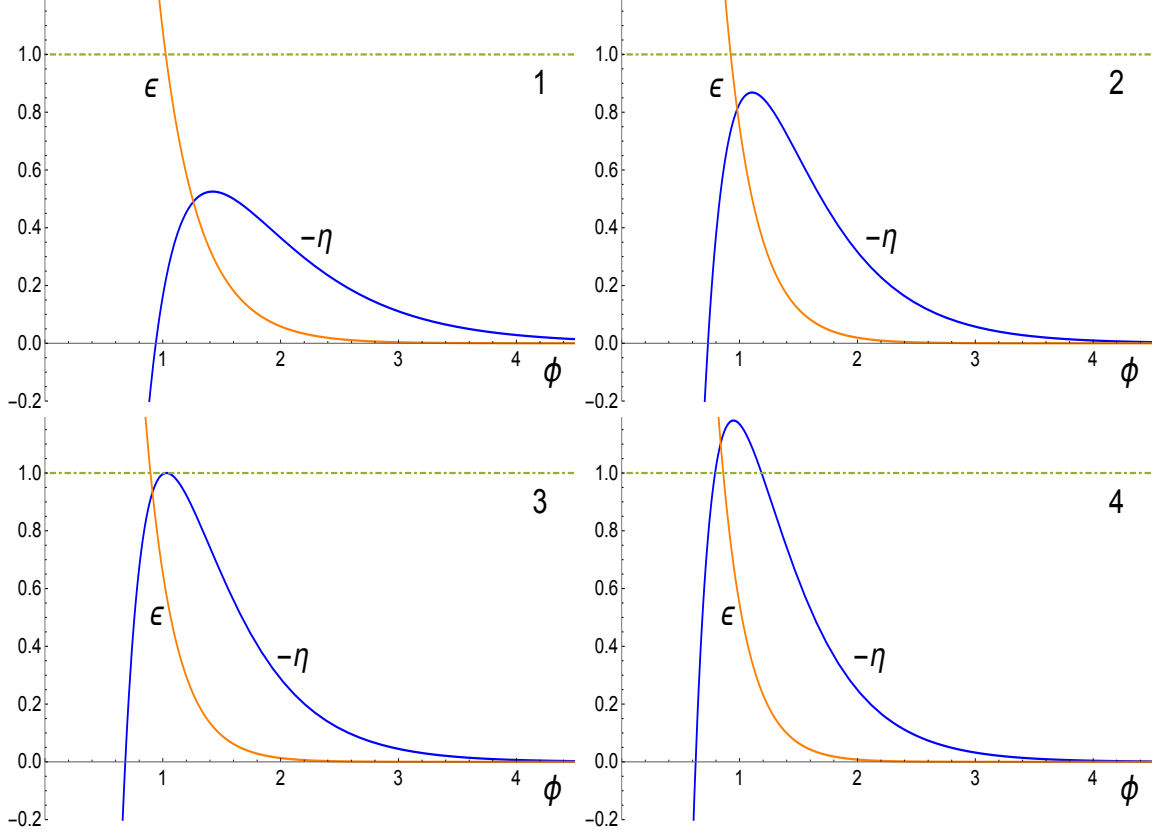


Figure 2: Plot of the slow-roll parameters ϵ and $-\eta$ as functions of the inflaton ϕ for values of λ smaller than λ_l (panels 1 and 2) for $\lambda = \lambda_l$ (panel 3) and for $\lambda > \lambda_l$. We see in panel 3 how slow-roll is terminated by the saturation of the condition $\eta = -1$ to briefly reset slow-roll and finally ending inflation by the condition $\epsilon = 1$ (see Fig. 3 below).

and

$$N_e \equiv \frac{1}{2p\lambda^2} \cosh^2 \left(\lambda \frac{\phi_e}{M_{pl}} \right). \quad (2.7)$$

2.1 Slow-roll interruptus

An interesting phenomenon occurs near the end of inflation and we illustrate it below for the case $p = 2$. By looking at the third panel in Fig. 2 (in Fig. 2 we plot $-\eta$) we see that the curve $-\eta$ just touches the horizontal line at 1 for $\lambda = \lambda_l$. This means that the condition $\eta = -1$ has been marginally satisfied signaling the end of slow-roll. In the Fig. 3 this detail is amplified together with a second curve for $-\eta$ corresponding to a value slightly greater than λ_l ($\lambda = 0.966$). We can see that at the point $a = (1.0374, 1)$ the condition $-\eta = 1$ is saturated but the curve enters again the region $-\eta < 1$ at $b = (1.0245, 1)$ when ϵ is still less than 1 i.e., slow-roll resets to eventually end inflation at $c = (0.8956, 1)$ when ϵ is finally equal to one.

In Fig. 3 we also show the potential for $\lambda \geq \lambda_l$ during this phenomenon: the small box under the number 1 in Fig. 3 shows the region during which slow-roll has ended and in the square above 2 the region where slow-roll is restored to eventually end permanently in the l.h.s. corner of the square corresponding to $\epsilon = 1$. The total number of e-folds between points

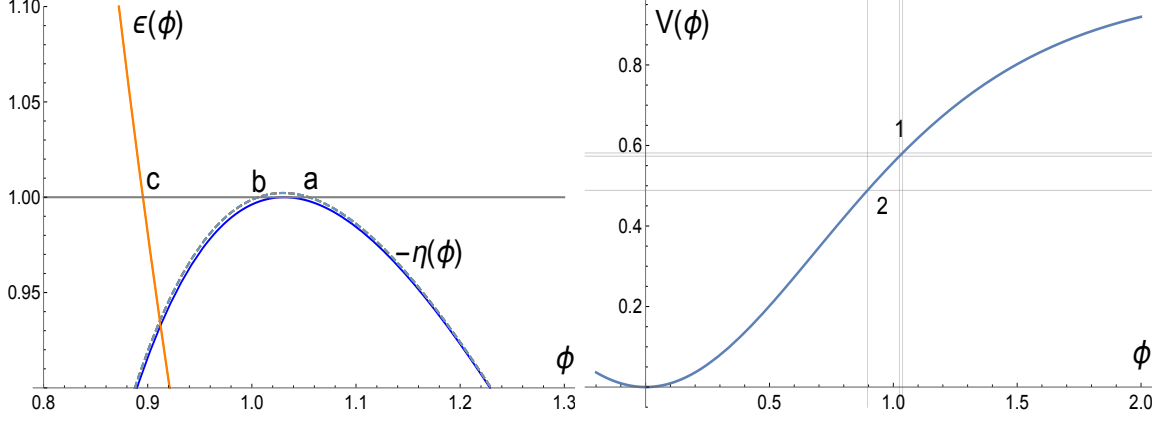


Figure 3: The l.h.s figure shows $-\eta$ for $\lambda = \lambda_l$ (bottom curve) (see Fig. 2 panel 3) and for a slightly larger value of λ . We see how the upper curve reaches the condition $-\eta = 1$ at the point a to reenter again at b the region where both $-\eta$ and ϵ are less than one resetting slow-roll to finally end inflation when $\epsilon(\phi) = 1$ at the point c . We also show the potential (for $\lambda \geq \lambda_l$) in the r.h.s figure where the very small box under the number 1 shows the region where slow-roll has ended and in the square above 2 the region where slow-roll is restored to eventually end inflation permanently in the l.h.s. corner of the large square corresponding to $\epsilon = 1$.

b and c is 0.104 corresponding to an 11% increase of the size of the universe in b . For slightly higher values of λ slow-roll will be interrupted for a longer period. While the number of e-folds after slow-roll is restored is negligible, the phenomenon itself is interesting and worth reporting.

2.2 The case $\lambda \geq \lambda_l$

The equations for N_k and N_e , Eqs. (2.6) and (2.7) respectively, are obtained by substituting ϕ_k and $\phi_{e\eta}$ from (2.1) and (2.2). Together with the large λ expansion they are given by

$$N_k = \frac{\delta_{n_s} + 4p\lambda^2 + \sqrt{\delta_{n_s}^2 + 4p^2\lambda^2\delta_{n_s} + 16p^2\lambda^4}}{4p\lambda^2\delta_{n_s}} = \frac{2}{\delta_{n_s}} + \frac{p+2}{8p\lambda^2} + \dots, \quad (2.8)$$

and

$$N_e = \frac{1 + 2p\lambda^2 + \sqrt{1 + 4p^2\lambda^2(\lambda^2 - 1)}}{4p\lambda^2} = 1 - \frac{p-1}{4p\lambda^2} + \dots. \quad (2.9)$$

We see that both terms are λ -independent for infinitely large λ , the term associated with the end of slow-roll is negligible contributing with less than 1 e-fold. We will see in Subsection 2.3 that when λ is small this is not the case and N_e is important.

Using Eqs. (2.8) and (2.9), the number of e-folds N_{ke} can be written in terms of the observable n_s as follows

$$N_{ke\eta}(n_s, \lambda, p) = \frac{2p(2 - \delta_{n_s})\lambda^2 + \sqrt{\delta_{n_s}^2 + 4p^2\lambda^2\delta_{n_s} + 16p^2\lambda^4} - \delta_{n_s}R_1}{4p\lambda^2\delta_{n_s}}, \quad (2.10)$$

where $R_1 = \sqrt{1 + 4p^2\lambda^2(\lambda^2 - 1)}$ and the subindex η appears here to remind us that N_{ke} is obtained from the solution to the $\eta = -1$ condition but then it is dropped (as well as the

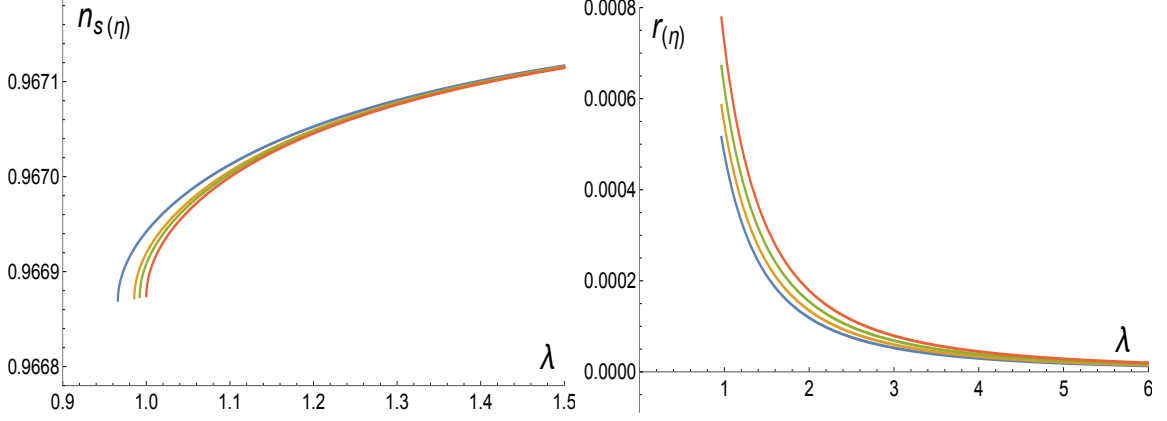


Figure 4: The l.h.s. figure illustrates the scalar spectral index n_s as a function of λ as given by Eq. (2.12) for $N_{ke} = 60$ and (from left to right) $p = 2, 3, 4, 10^6$ while the r.h.s. figure shows $r_{(\eta)}(\lambda)$ given by Eq. (2.16) for $p = 2$ and (from left to right) $N_{ke} = 64, 60, 56, 52$, both figures with $\lambda > \lambda_l$. There is no appreciable change in $r_{(\eta)}$ when plotted for various values of p . The subindex η is intended to emphasize that the solution has been obtained under the condition $\eta = -1$ for ending slow-roll.

argument) from the following expressions. For large λ , N_{ke} has the following expansion

$$N_{ke} = \frac{2 - \delta_{n_s}}{\delta_{n_s}} + \frac{3}{8\lambda^2} - \frac{8 - 4\delta_{n_s} - p^2(8 - \delta_{n_s})}{128p^2\lambda^4} + \dots \quad (2.11)$$

Thus, N_{ke} is p -independent for infinitely large λ . We can solve Eq. (2.10) for n_s in terms of N_{ke} (see Fig. 4)

$$n_s = \frac{1 + 4p^2\lambda^2 - (R_1 - 2(3 - 2N_{ke})p\lambda^2)(R_1 + 2(1 + 2N_{ke})p\lambda^2)}{1 - (R_1 + 2(1 + 2N_{ke})p\lambda^2)^2} \quad (2.12)$$

Thus, the leading order term in the large- N_{ke} expansion of the scalar spectral index n_s is also p -independent

$$n_s = 1 - \frac{2}{N_{ke}} + \left(1 + \frac{2R_1 - p}{4p\lambda^2}\right) \frac{1}{N_{ke}^2} + \dots, \quad (2.13)$$

for the mean value $n_s = 0.9649$ [16] Eq. (2.13) implies $N_{ke} \approx 57$.

One can notice that N_{ke} as given by Eq. (2.10) above depends only on the observable n_s , this is so because ϕ_k was obtained by solving the equation (1.4) written in the form $\delta_{n_s} + 2\eta - 6\epsilon = 0$. We could also obtain ϕ_k by solving Eq. (1.5) or $r = 16\epsilon$ and write an equivalent expression for N_{ke} involving only the observable r with the result

$$\cosh^2\left(\lambda \frac{\phi_k}{M_{pl}}\right) = \frac{1}{2} \left(1 + \sqrt{1 + \frac{32p^2\lambda^2}{r}}\right), \quad (2.14)$$

which together with Eq. (2.2) implies that the number of e-folds can now be written as

$$N_{ke\eta}(r, \lambda, p) = \frac{-2p\lambda^2 + \sqrt{1 + \frac{32p^2\lambda^2}{r}} - R_1}{4p\lambda^2} \quad (2.15)$$

Solving for r

$$r = \frac{8p}{p(-1 + 2(1 + 2N_{ke}(1 + N_{ke}))\lambda^2) + (1 + 2N_{ke}R_1)} , \quad (2.16)$$

as shown by Fig. 4 for the $p = 2$ case and for various values of N_{ke} . In the large- N_{ke} limit r is given by

$$r = \frac{2}{\lambda^2 N_{ke}^2} - \frac{2p\lambda^2 + R_1}{p\lambda^4 N_{ke}^3} + \dots . \quad (2.17)$$

2.3 The case $\lambda < \lambda_l$

The end of inflation is given by the solution to the condition $\epsilon = 1$

$$\cosh^2 \left(\lambda \frac{\phi_{e\epsilon}}{M_{pl}} \right) = \frac{1}{2} \left(1 + \sqrt{1 + 2p^2\lambda^2} \right) , \quad (2.18)$$

while ϕ_k in terms of n_s is given, as before, by Eq. (2.1).

The equations for N_k and N_e , Eqs. (2.6) and (2.7) respectively, and their small λ expansion, are given by

$$N_k = \frac{\delta_{n_s} + 4p\lambda^2 + \sqrt{\delta_{n_s}^2 + 4p^2\lambda^2\delta_{n_s} + 16p^2\lambda^4}}{4p\lambda^2\delta_{n_s}} = \frac{1}{2p\lambda^2} + \frac{p+2}{2\delta_{n_s}} - \frac{p(p^2-4)\lambda^2}{2\delta_{n_s}^2} + \dots , \quad (2.19)$$

and

$$N_e = \frac{1 + \sqrt{1 + 2p^2\lambda^2}}{4p\lambda^2} = \frac{1}{2p\lambda^2} + \frac{p}{4} - \frac{p^3\lambda^2}{8} + \dots . \quad (2.20)$$

For small λ the first term in the expansion of N_k grows large thus, (contrary to the large λ case where N_e is less than 1) here the end of inflation is important and necessary to cancel the leading term in N_k so that the number of e-folds of inflation goes like $N_{ke} \approx (p+2)/2\delta_{n_s}$, to first approximation.

The number of e-folds Eq. (2.5) is

$$N_{ke\epsilon}(n_s, \lambda, p) = \frac{4p\lambda^2 - \delta_{n_s}R_2 + \sqrt{\delta_{n_s}^2 + 4p^2\lambda^2\delta_{n_s} + 16p^2\lambda^4}}{4p\lambda^2\delta_{n_s}} , \quad (2.21)$$

where $R_2 = \sqrt{1 + 2p^2\lambda^2}$ and, in analogy with Eq. (2.10), the subindex ϵ appears here to remind us that N_{ke} is obtained from the solution to the $\epsilon = 1$ condition but then it is dropped from the following expressions. From Eq. (2.21) we can solve for n_s (see Fig. 5)

$$n_s = \frac{1 + 4p^2\lambda^2 - (R_2 + 4(-2 + N_{ke})p\lambda^2)(R_2 + 4N_{ke}p\lambda^2)}{1 - (R_2 + 4N_{ke}p\lambda^2)^2} , \quad (2.22)$$

for large N_{ke}

$$n_s = 1 - \frac{2}{N_{ke}} + \frac{2R_2 - p}{4p\lambda^2 N_{ke}^2} + \dots . \quad (2.23)$$

To obtain N_{ke} in terms of r we proceed in a similar way as in Eq. (2.16). From Eqs. (2.5), (2.14) and (2.3) we get

$$N_{ke\epsilon}(r, \lambda, p) = \frac{\sqrt{r + 32p^2\lambda^2} - \sqrt{r}\sqrt{1 + 2p^2\lambda^2}}{4p\lambda^2\sqrt{r}} , \quad (2.24)$$

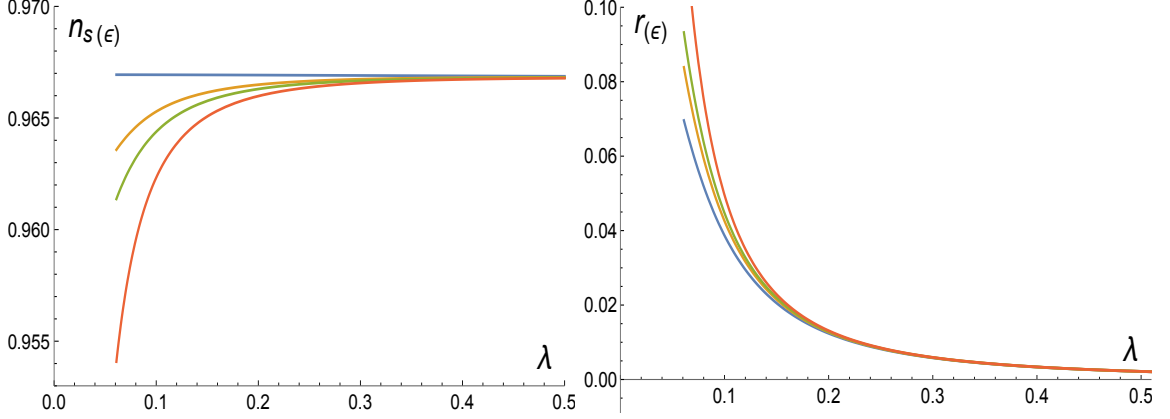


Figure 5: The l.h.s. figure illustrates the scalar spectral index n_s as a function of λ as given by Eq. (2.22) for $N_{ke} = 60$ and (from top to bottom) $p = 2, 3, 4, 10^6$ while the r.h.s. figure shows $r_{(\epsilon)}(\lambda)$ given by Eq. (2.25), also for $N_{ke} = 60$ and (from left to right) $p = 2, 3, 4, 10^6$, both for $\lambda < \lambda_l$. The subindex ϵ is intended to emphasize that the solution has been obtained under the condition $\epsilon = 1$ for ending inflation.

solving for r (see Fig. 5)

$$r = \frac{16p}{p + 8N_{ke}^2 p \lambda^2 + 4N_{ke} \sqrt{1 + 2p^2 \lambda^2}}, \quad (2.25)$$

with large N_{ke} expansion

$$r = \frac{2}{\lambda^2 N_{ke}^2} - \frac{\sqrt{1 + 2p^2 \lambda^2}}{p \lambda^4 N_{ke}^3} + \dots. \quad (2.26)$$

The previous results for n_s in the large N_{ke} expansion Eqs. (2.13) and (2.23) give a leading term $n_s = 1 - \frac{2}{N_{ke}} + \dots$. Also Eqs. (2.17) and (2.26) give a leading term $r = \frac{2}{\lambda^2 N_{ke}^2} + \dots$ for the large N_{ke} expansion of r .

3 Removing the λ and V_0 parameters

We can express the parameter λ purely in terms of p and the observables n_s and r by substituting e.g., ϕ_k from Eq. (2.1) in Eq. (1.5), $r = 16\epsilon$, and solving for λ

$$\lambda = \frac{\sqrt{p^2(8\delta_{n_s} - r)^2 - 4r^2}}{8p\sqrt{2r}}. \quad (3.1)$$

Technically, the parameter λ can take values from 0 to ∞ . The limiting value $\lambda = 0$ occurs for $r = \frac{8p}{p+2}\delta_{n_s}$ or, equivalently, $n_s = 1 - \frac{p+2}{8p}r$ which is exactly the relation between n_s and r for monomial potentials of the form $V(\phi) \sim \phi^p$. Clearly $\lambda \rightarrow \infty$ when $r \rightarrow 0$.

The limiting value λ_l , defined by Eq. (2.4), distinguishes between ending slow-roll by $\eta = -1$ or $\epsilon = 1$. For λ given by (3.1) above, λ_l translates into a limiting value for r , for a fixed value of n_s , as follows

$$r_l = \frac{8p}{p^2 - 4} \left(4\sqrt{p^2 - 1} + p(4 + \delta_{n_s}) - 2\sqrt{2p(4 + \delta_{n_s})(p + \sqrt{p^2 - 1}) + \delta_{n_s}^2 - 4} \right), \quad (3.2)$$

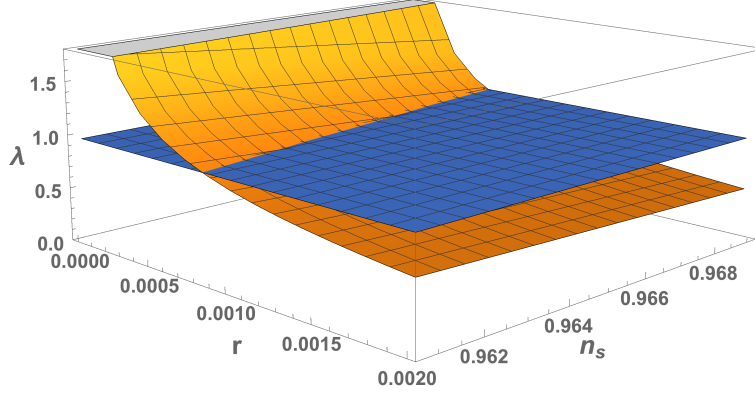


Figure 6: Plot of the parameter λ as given by Eq. (3.1) for $p = 2$ as a function of n_s and r . The horizontal plane shows the limiting value λ_l of Eq. (2.4) which separates the parameter region where $\eta = -1$ ends slow-roll ($\lambda > \lambda_l$) from the region where inflation is terminated by the $\epsilon = 1$ condition ($\lambda < \lambda_l$). These conditions on λ are translated in conditions on r for a fixed value of n_s (see Eq. (3.2)).

thus,

$$\lambda \geq \lambda_l \iff r \leq r_l, \quad \lambda < \lambda_l \iff r > r_l. \quad (3.3)$$

When $p = 2$ we have

$$r_l = \frac{4\delta_{n_s}^2}{4 + 2\sqrt{3} + \delta_{n_s}}, \quad (3.4)$$

the case $p = 2$ implies $r_l = (6.7 \pm 1.6) \times 10^{-4}$ for $n_s = 0.9649 \pm 0.0042$ [16]. When the condition $\eta = -1$ is met $\lambda \geq \lambda_l$, and r should be less than r_l while values of r larger than r_l correspond to $\lambda < \lambda_l$ which occur when the condition $\epsilon = 1$ ends inflation (see Fig. 6) thus, the condition $\eta = -1$ is only satisfied for small values of r . For example, for $p \geq 1$ the largest value of r_l is $r_l \approx 1.53 \times 10^{-3}$ which occurs for $n_s = 0.9607$ while for $p \geq 2$ the largest value is $r_l \approx 8.23 \times 10^{-4}$ also at $n_s = 0.9607$.

For small r , λ has the following expansion

$$\lambda = \frac{\delta_{n_s}}{\sqrt{2r}} - \frac{\sqrt{r}}{8\sqrt{2}} - \frac{r^{3/2}}{32\sqrt{2}p^2\delta_{n_s}} + \dots, \quad (3.5)$$

thus, to leading order in r , λ is p -independent. However, from the bounds $n_s = 0.9649 \pm 0.0042$ and $r < b$, the parameter λ is bounded from below as $\lambda > \frac{1}{16\sqrt{2}b} \sqrt{4(8(n_s^u - 1) + b)^2 - b^2}$ where n_s^u is the upper bound for n_s . For the current bounds $n_s^u = 0.9691$ and $b = 0.063$, a lower bound for λ is implied as $\lambda > 0.061$.

3.1 General solutions for $r(n_s, N_{ke}, p)$

We can eliminate the parameter λ in all the previous equations in such a way that only the observables n_s and r appear. First we separately discuss the $p = 2$ case by substituting λ from Eq. (3.1) into the expressions for N_{ke} given by Eqs. (2.10), (2.15), (2.21), (2.24) and solving for r obtaining the following *two* independent solutions: one for the case $\lambda \geq \lambda_l$ where the end of slow-roll is given by the condition $\eta = -1$ and labeled by the symbol η and one for the case $\lambda < \lambda_l$ where the end of inflation is given by the condition $\epsilon = 1$, labeled by the

symbol ϵ

$$r_\eta(p=2) = \frac{4(N_{ke}\delta_{n_s}-2)((N_{ke}+1)\delta_{n_s}-2)}{N_{ke}((N_{ke}+1)\delta_{n_s}-2)-3}, \quad (3.6)$$

$$r_\epsilon(p=2) = \frac{4(N_{ke}\delta_{n_s}-2)^2}{N_{ke}(N_{ke}\delta_{n_s}-2)+1}. \quad (3.7)$$

The approximations for large N_{ke} are (see Figs. 7 and 8 for the $p=2$ case).

$$r_\eta(p=2) = \frac{4(N_{ke}\delta_{n_s}-2)}{N_{ke}} + \frac{12}{N_{ke}^2} + \dots, \quad (3.8)$$

$$r_\epsilon(p=2) = \frac{4(N_{ke}\delta_{n_s}-2)}{N_{ke}} - \frac{4}{N_{ke}^2} + \dots. \quad (3.9)$$

For $p \neq 2$ we can proceed in an analogous way as above and solving in each case for r in terms of p , N_{ke} and δ_{n_s} obtaining the following two independent solutions

$$r_\eta = \frac{8p}{N_{ke}(N_{ke}+1)(p^2-4)} (p(N_{ke}((N_{ke}+1)\delta_{n_s}-2)-3) + R_3), \quad (3.10)$$

where $R_3 = (9p^2 + 4N_{ke}((N_{ke}+1)\delta_{n_s}-2)(-2-p^2 + N_{ke}((N_{ke}+1)\delta_{n_s}-2)))^{1/2}$ and

$$r_\epsilon = \frac{8p}{N_{ke}^2(p^2-4)} (p(N_{ke}(N_{ke}\delta_{n_s}-2)+1) - R_4), \quad (3.11)$$

where $R_4 = (p^2 + 2N_{ke}(N_{ke}\delta_{n_s}-2)(2N_{ke}(N_{ke}\delta_{n_s}-2)+p^2))^{1/2}$. Approximations for large N_{ke} are as follows

$$r_\eta = \frac{8p}{p-2} \frac{(N_{ke}\delta_{n_s}-2)}{N_{ke}} - \frac{8p(p-1)}{p-2} \frac{1}{N_{ke}^2} + \dots, \quad (3.12)$$

$$r_\epsilon = \frac{8p}{p-2} \frac{(N_{ke}\delta_{n_s}-2)}{N_{ke}} - \frac{4p^2}{p+2} \frac{1}{N_{ke}^2} + \dots, \quad (3.13)$$

We expect the first term to dominate and should be positive thus, for $p > 2$, $n_s < 1 - 2/N_{ke}$ while $p < 2$ requires $n_s > 1 - 2/N_{ke}$ or, perhaps more appropriate, for $p > 2$, $N_{ke} > \delta_{n_s}/2$ while $p < 2$ requires $N_{ke} < \delta_{n_s}/2$. From the Planck bounds $n_s = 0.9649 \pm 0.0042$ it follows that $50.9 < N_{ke} < 64.7$ for any p . For a dominant first term we also expect that $r < b$ where $b = 0.063$ is the upper bound for r reported by the Planck 2018 Collaboration [16]. Thus assuming that

$$r \approx \frac{8p}{p-2} \frac{(N_{ke}\delta_{n_s}-2)}{N_{ke}} < b, \quad (3.14)$$

we get

$$p > \frac{2bN_{ke}^l}{16 + N_{ke}^l(b - 8(1 - n_s^u))} \approx 0.97, \quad (3.15)$$

where $N_{ke}^l \approx 50.9$ is the lower bound for N_{ke} and $n_s^u \approx 0.9691$ is the upper bound for n_s . The tensor-to-scalar ratio r is determined at ϕ_k thus, we conclude that p should be bigger than ≈ 0.97 at the scale of wavenumber mode k .

For the $p=2$ case, the bound $\lambda \geq \lambda_l = (2 + \sqrt{3})^{1/2}/2 \approx 0.9659$ is equivalent to a bound on r as $r < 0.00082$ for $n_s = 0.9607$. Thus, the expression for r_η is valid for very small r only. In this regime the solution r_ϵ (which should be used for $\lambda < \lambda_l$ or $r > r_l \approx 0.00051$ at

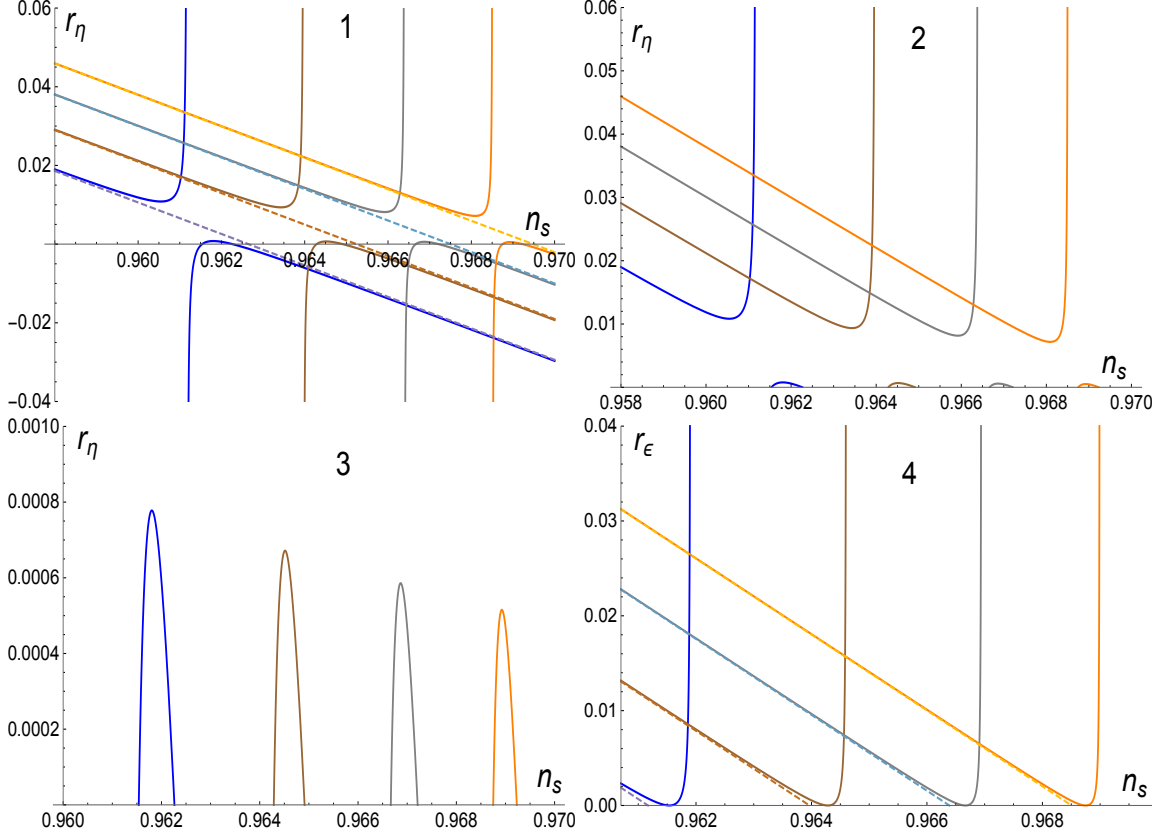


Figure 7: In panel 1 we plot the solution for r as a function of n_s for $p = 2$ and (from left to right) $N_{ke} = 52, 56, 60$ and 64 (Eq. (3.6)). Dashed lines correspond to the large N_{ke} approximation given by Eq. (3.8). The negative part of the solutions as well as the approximations are discarded in panel 2. The very small bumps in panel 2 are the relevant solutions because r_η is only valid for small r (less than ≈ 0.00082 for the $p = 2$ case). This bumps are amplified in panel 3 and from them only the l.h.s. part of the curve is the solution which matters, because it connects smoothly with the r_ϵ solution shown in panel 4. Because r_ϵ and its approximation as given by Eqs. (3.7) and (3.9) are valid for larger values of r ($\lambda < \lambda_l$) and because they are very close to the r_η solution in the small r regime (large λ) it is then possible to use the solution r_ϵ of (3.7) for the whole range of r with negligible error in the very small r regime. Thus, the (finally) relevant solution can be considered as the part of r_ϵ in panel 4 which ascend almost vertically from $r = 0$ to end in the monomials as shown in Fig. 8 for $p = 2$, $N_{ke} = 50, 60$ and for other values of p in Fig. 10 where we plot Eq. (3.11).

$n_s = 0.9691$) is very close to the r_η solution being possible to use it also for the very small r regime (large λ regime) with negligible error. The case $p \neq 2$ is not very different thus, in what follows, we study only the r_ϵ solution for all possible values of r . In Fig. 7 we show the solutions (3.6) and (3.7) for the $p = 2$ case reproducing in Fig. 8 the numerical solution which appear in Fig. 8 of the Planck 2018 Collaboration [16] (shown here as Fig. 9). This solution contains the monomial solution for $r(n_s)$ of the ϕ^2 model. In Fig. 10 we plot several other cases of Eq. (3.11) by giving p the values $p = 2, 4/3, 1$ and $2/3$ containing all the monomial solutions shown in Fig. 9. These solutions are contained exactly in the α -attractor models as shown analytically in the following subsection.

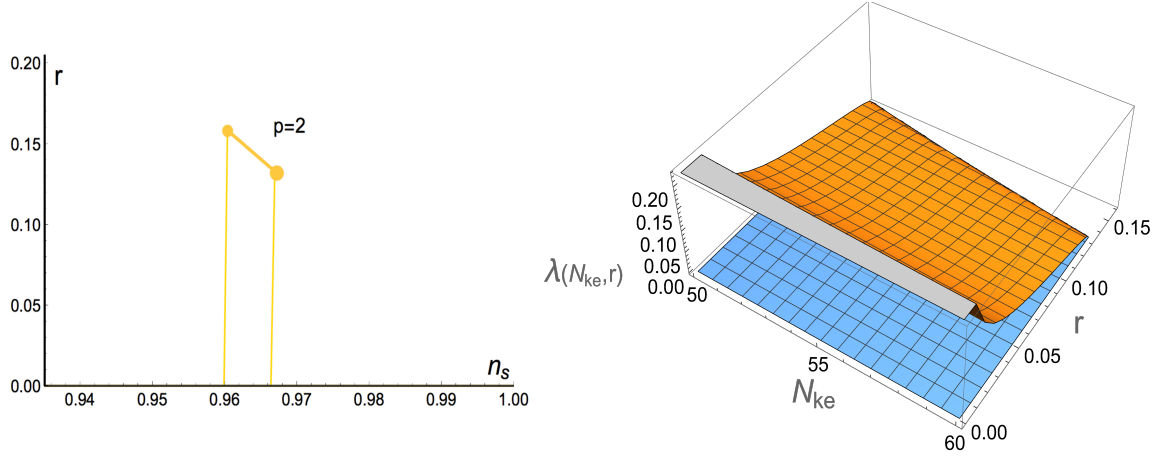


Figure 8: In the l.h.s. figure we plot r as a function of n_s as given by Eq. (3.7) for $p = 2$, $N_{ke} = 50$ (joining the small circle) and $N_{ke} = 60$ reproducing the numerical calculation shown in the Fig. 8 of the Planck 2018 Collaboration [16] and duplicated here below as Fig. 9. The r.h.s. figure is a similar plot with a trivial extension in the N_{ke} direction. The horizontal plane is just for reference to the $\lambda = 0$ limiting value.

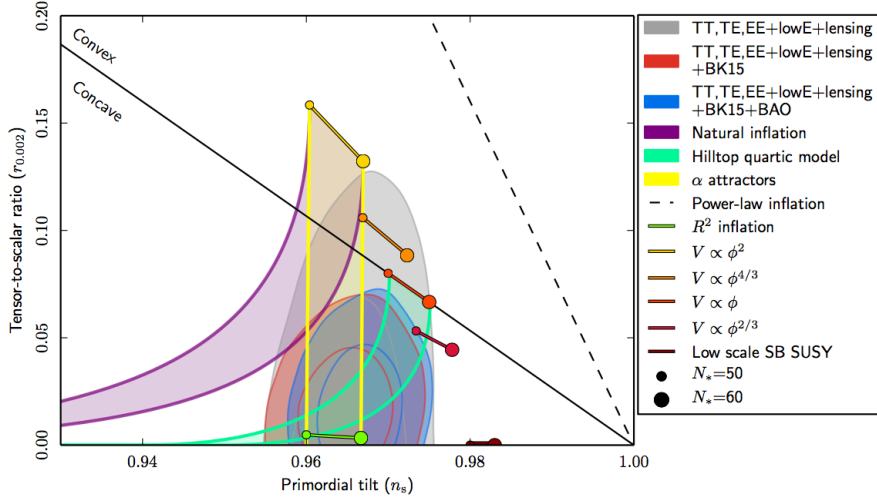


Figure 9: We take figure 8 of the Planck Collaboration 2018 article [16] where monomial potentials are also considered together with several other interesting models of inflation (see description in the right hand side panel of the figure). From the figure we see that there is a substantial overlap of the predictions of α -attractor inflation (yellow, almost vertical curves for the $p = 2$ case) with Planck alone and in combination with BICEP2/Keck Array (BK15) [35] or BICEP2/Keck Array+Baryon Acoustic Oscillations (BK15+BAO) data. For other values of p compare with the plot of Eq. (3.11) in Fig. 10 below.

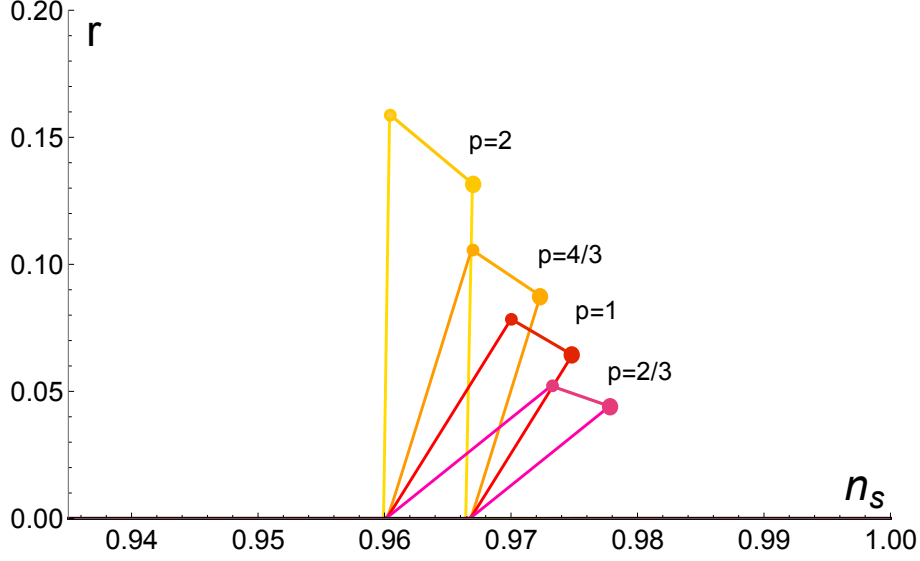


Figure 10: Plot of r_ϵ as given by Eqs. (3.7) and (3.11) as a function of n_s for $N_{ke} = 50$ (joining the small circles) and $N_{ke} = 60$ for $p = 2, 4/3, 1$ and $2/3$ as shown, appearing in the Fig. 8 of the Planck 2018 Collaboration and duplicated here as Fig. 9 above. We see how the α -attractor solutions practically cover the entire region of Planck alone and in combination with BK15 or BK15+BAO data.

3.2 Monomials as particular cases of α -attractors

For monomials of the form $V_{mon} = \frac{1}{2}m^{4-p}\phi^p$ we get $\phi_k = \frac{2\sqrt{2}p}{\sqrt{r}}$ and $\phi_e = \frac{p}{\sqrt{2}}$ from where it follows that

$$r = \frac{16p}{4N_{ke} + p}, \quad (3.16)$$

also

$$\delta_{n_s} = \frac{p+2}{8p}r. \quad (3.17)$$

Eqs. (3.16) and (3.17) follow from the condition $\epsilon = 1$, this condition ends inflation whenever $2/3 \leq p \leq 2$. For p outside this range slow-roll is terminated by $\eta = -1$ for $p < 2/3$ in which case $r = 8p/(2N_{ke} + p - p^2)$ or $\eta = +1$ for $p > 2$ in this case $r = 8p/(2N_{ke} + p - 1)$. In any case for large N_{ke} and $p \ll N_{ke}$ they all have the same limit $\sim 4p/N_{ke}$. Thus for $p = 2$ and $N_{ke} = 50$, $(n_s, r) = (\frac{97}{101}, \frac{16}{101}) \approx (0.9604, 0.1584)$ and so on. In this way we can calculate all the points appearing as circles in Fig. 9. The point $(0.9604, 0.1584)$, for example, is reached by the solution $r_\epsilon(p = 2)$ Eq. (3.7) for $N_{ke} = 50$ as shown by the left line in Fig. 8 and similarly for the $N_{ke} = 60$ line on the r.h.s. For $p \neq 2$ Eq. (3.11) applies. In this way we draw Fig. 10 connecting the α -attractor T-models with all the monomial as shown. Analytically, we can see this as follows: for the $p = 2$ case we substitute Eq. (3.17) in Eq. (3.7) and we get $r_\epsilon(p = 2) = 16/(2N_{ke} + 1)$ which is Eq. (3.16) (with $p = 2$). In general (for $p \neq 2$)

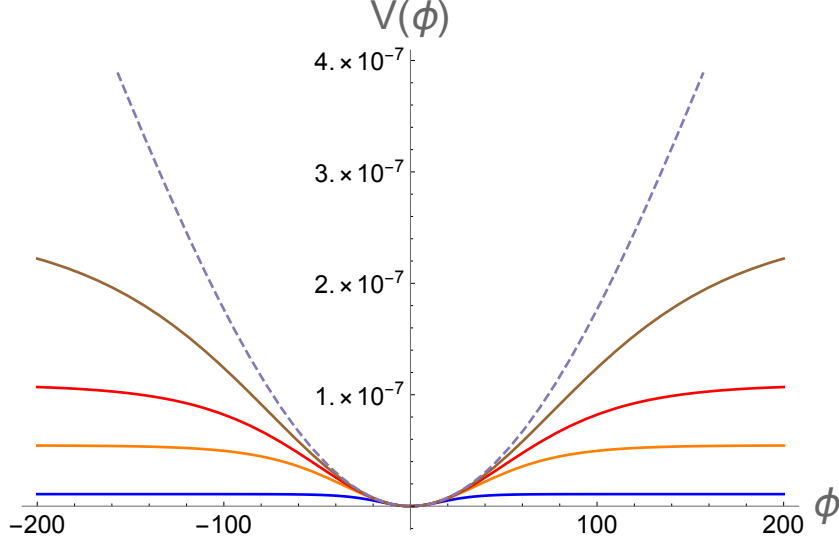


Figure 11: Plot of the α -attractor potential as given by Eq. (3.19) as a function of ϕ for $p=2$ and $\delta_{n_s} = 0.0351$ (equivalently $n_s = 0.9649$) and various values of r reaching $r = 8p\delta_{n_s}/(p+2)$ (dashed curve) signaling the transition of the $\tanh^p(\lambda\phi)$ potential (3.19) to the monomial ϕ^p potential given by Eq. (3.20). The fact that the attractors end in monomials is now easily understood because the attractor potential transitions to the monomials potential when $\lambda = 0$, that is, when $r = 8p\delta_{n_s}/(p+2)$ which is precisely the relation between r and n_s for the monomials potential.

substituting Eq. (3.17) in Eq. (3.11) gives

$$r_\epsilon = \frac{16p}{4N_{ke} + p}, \quad (3.18)$$

which is Eq. (3.16), exactly. Thus, all the monomial models are contained as particular cases by the α -attractor T-models. This is illustrated by Fig. 10 only for the monomials shown in Fig. 8 (reproduced here as Fig. 9) of the Planck 2018 Collaboration [16]. Even more to the point: *the monomials are the ending points of the attractors* [6]. This can be seen as follows: if we substitute Eq. (3.17) in the equation defining λ (Eq. (3.1)) we find that $\lambda = 0$ becoming imaginary after this point. To have a clear understanding of this phenomenon let us substitute equation (3.1) for λ in Eq. (1.1); the resulting potential can then be written as

$$V = \frac{3}{2}A_s\pi^2r \left(\frac{\sqrt{p(8\delta_{n_s} - r) + 2r}}{\sqrt{p(8\delta_{n_s} - r) - 2r}} \right)^p \tanh^p \left(\frac{\sqrt{p^2(8\delta_{n_s} - r)^2 - 4r^2}}{8p\sqrt{2r}}\phi \right), \quad (3.19)$$

where V_0 has been calculated from Eq. (1.6). If we study the potential (3.19) in the limit where $\delta_{n_s} \rightarrow \frac{p+2}{8p}r$ we find that it reduces to the following expression

$$V_{mon} = \frac{3}{2}A_s\pi^2r \left(\frac{r}{8p^2} \right)^{p/2} \phi^p. \quad (3.20)$$

One can easily check that the potential (3.20) corresponds exactly to monomials of the form $V_{mon} = \frac{1}{2}m^{4-p}\phi^p$. Thus, the fact that we reach the monomials in Fig. 10 is now easily understood because our original potential transitions to the monomials potential when $\lambda = 0$,

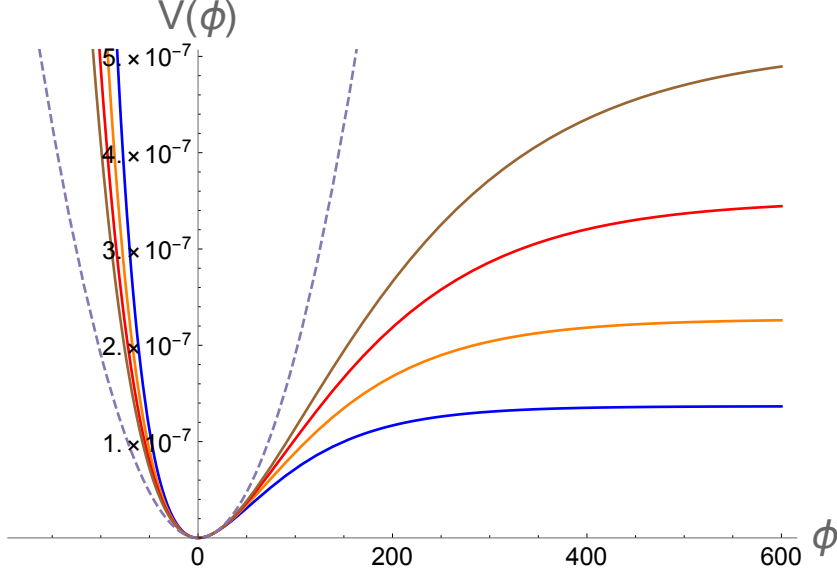


Figure 12: As for the T-models the α -attractor E-models also join and end in monomials much in the same way as T-models do. Here we show the potential as given by Eq. (3.21) as a function of ϕ for $p=2$, $\delta_{n_s} = 0.0351$ (equivalently $n_s = 0.9649$) and various values of r reaching $r = 8p\delta_{n_s}/(p+2)$ (dashed curve) signaling the transition of the potential (3.21) to the monomials $V_{mon} = \frac{1}{2}m^{4-p}\phi^p$ potential, given by Eq. (3.20) in terms of the observable r .

that is, when $r = 8p\delta_{n_s}/(p+2)$ which is precisely the relation between r and n_s for the monomials potential. The potential (3.19) is shown in Fig. 11 as a function of ϕ for $p = 2$ and the mean value $n_s = 0.9649$ [16] (or $\delta_{n_s} = 0.0351$) for various values of r reaching $r = 8p\delta_{n_s}/(p+2)$ (dashed curve) signaling the transition of the $\tanh^p(\lambda\phi)$ potential (3.19) to the monomial ϕ^p potential of Eq. (3.20). The expression $r = 8p\delta_{n_s}/(p+2)$ makes $\lambda = 0$ but $\lambda = 0$ in what we saw before takes us to the ends of the curves in Fig. 10 reaching the predictions in the n_s - r plane for the monomials potential. A similar study can be done with α -attractor E-models defined by the potential (1.2) which generalize the Starobinsky potential in the Einstein frame. In this case the generalized potential written in terms of n_s and r

$$V = \frac{3}{2}A_s\pi^2r \left(\frac{p(8\delta_{n_s} - r)}{8p\delta_{n_s} - (p+2)r} \right)^p \left(1 - e^{-\frac{8p\delta_{n_s} - (p+2)r}{4p\sqrt{2}r}\phi} \right)^p, \quad (3.21)$$

also contains the monomials potential (3.20) much in the same way as discussed before (see Fig. 12).

4 Conclusions

We have carried out an analytical study of a class of α -attractor T-models generalized from the simplest monomials and given by the potential $V = V_0 \tanh^p \left(\lambda \frac{\phi}{M_{pl}} \right)$ without paying attention to its origin, but dealing with it only as a phenomenological model of inflation. We can see how the analytical study clarifies several of its important properties and characteristics. In particular, we have obtained exact solutions, valid for any p , for the spectral index n_s and for the tensor-to-scalar ratio r in terms of the number of e-folds N_{ke} and the parameter λ .

Eliminating the parameter λ we can also obtain exact solutions for r in terms of n_s and N_{ke} . These solutions allow us to study the n_s - r plane and compare with numerical studies such as those presented by the Planck Collaboration, reproducing their results. Our analytical study allows us to observe precisely how the monomial potentials are contained in the α -attractor models and also constitute the end points of our solutions. Finally we show how in the appropriate limit the potential for the α -attractor for both T and E-models exactly reduces to the monomials potential providing a clear explanation of the relationship between them.

Acknowledgments

I would like to thank the anonymous referee for a detailed and careful revision of the article and for useful advice. Financial support from UNAM-PAPIIT, IN104119, *Estudios en gravitación y cosmología* is gratefully acknowledged.

References

- [1] R. Kallosh and A. Linde. Universality Class in Conformal Inflation. *JCAP*, **07**(2013)002.
- [2] D. Roest. Universality classes of inflation. *JCAP*, **01**(2014)007.
- [3] S. Ferrara, R. Kallosh, A. Linde and M. Porrati. Minimal Supergravity Models of Inflation. *Phys. Rev. D*, **88**(2013)8, 085038.
- [4] R. Kallosh and A. Linde. Non-minimal Inflationary Attractors. *JCAP*, **10**(2013)033.
- [5] R. Kallosh and A. Linde. Multi-field Conformal Cosmological Attractors. *JCAP*, **12**(2013)006.
- [6] R. Kallosh, A. Linde and D. Roest. Superconformal Inflationary α -Attractors. *JHEP*, **11**(2013)198.
- [7] R. Kallosh, A. Linde and D. Roest. Universal Attractor for Inflation at Strong Coupling. *Phys. Rev. Lett*, **112**(2014)1, 011303.
- [8] S. Cecotti and R. Kallosh. Cosmological Attractor Models and Higher Curvature Supergravity. *JHEP*, **05**(2014)114.
- [9] R. Kallosh, A. Linde and D. Roest. Large field inflation and double α -attractors. *JHEP*, **08**(2014)052.
- [10] R. Kallosh, A. Linde and D. Roest. The double attractor behavior of induced inflation. *JHEP*, **09**(2014)062.
- [11] M. Galante, R. Kallosh, A. Linde and D. Roest. Unity of Cosmological Inflation Attractors. *Phys. Rev. Lett*, **114**(2014)14, 141302.
- [12] J. J. M. Carrasco, R. Kallosh and A. Linde. α -Attractors: Planck, LHC and Dark Energy. *JHEP*, **10**(2015) 147.
- [13] J. J. M. Carrasco, R. Kallosh and A. Linde. Cosmological Attractors and Initial Conditions for Inflation. *Phys. Rev. D*, **92**(2015) 6, 063519.
- [14] J. J. M. Carrasco, R. Kallosh and A. Linde. Minimal supergravity inflation. *Phys. Rev. D*, **93**(2016)6, 061301.
- [15] R. Kallosh and A. Linde, D Roest and T. Wrase. Sneutrino inflation with α -attractors. *JCAP*, **11**(2016) 046.
- [16] Y. Akrami *et al.* [Planck Collaboration], Planck 2018 results. X. Constraints on inflation. *Astron. Astrophys.*, **641**(2020) A10, arXiv:1807.06211, [astro-ph.CO].

- [17] S. D. Odintsov and V. K. Oikonomou. Inflationary α -attractors from $F(R)$ gravity. *Phys. Rev. D*, **94**(2016)12, 124026.
- [18] Y. Ueno and K. Yamamoto. Constraining the general reheating phase in the α -attractor inflationary cosmology. *Phys. Rev. D*, **93**(2016)8, 083524.
- [19] K. S. Kumar, J. Marto, P. Vargas Moniz, and S. Das. Non-slow-roll dynamics in α -attractors. *JCAP*, **04**(2016) 005.
- [20] Eshaghi, M. Zarei, N. Riazi and A. Kiasatpour. CMB and reheating constraints to α -attractor inflationary models. *Phys. Rev. D*, **93**(2016)12, 123517.
- [21] A. Di Marco, P. Cabella and N. Vittorio. Constraining the general reheating phase in the α -attractor inflationary cosmology. *Phys. Rev. D*, **95**(2017)10, 103502.
- [22] N. Rashidi, K. Nozari. α -Attractor and reheating in a model with noncanonical scalar fields. *Int. J. Mod. Phys. D*, **27**(2018) 07, 1850076.
- [23] Y. Akrami, Yashar, R. Kallosh, A. Linde and V. Vardanyan. Dark energy, α -attractors, and large-scale structure surveys. *JCAP*, **06**(2018) 041.
- [24] I. Dalianis, A. Kehagias and G. Tringas. Primordial black holes from α -attractors. *JCAP*, **01**(2019) 037.
- [25] F. X. Linares Cedeño, A. Montiel, J. C. Hidalgo and G. Germán. Bayesian evidence for α -attractor dark energy models. *JCAP*, **08**(2019) 002.
- [26] R. Shojaei, K. Nozari and F. Darabi. α -Attractors and reheating in a non-minimal inflationary model. *Int. J. Mod. Phys. D*, **29**(2020) 010, 2050077.
- [27] S. D. Odintsov and V. K. Oikonomou Inflationary attractors in $F(R)$ gravity. *Phys. Lett. B*, **807**(2020) 135576
- [28] R. Shojaei, K. Nozari and F. Darabi. α -Attractors and reheating in a class of Galileon inflation. *Int. J. Mod. Phys. D*, **30**(2021) 05, 2150036.
- [29] E.V. Linder. Dark energy from α -attractors. *Phys. Rev. D*, **91**(2015)12, 123012.
- [30] K. Dimopoulos, C. Owen. Quintessential Inflation with α -attractors. *JCAP*, **06**(2017) 027.
- [31] K. Dimopoulos and D. Woo. Instant preheating in quintessential inflation with α -attractors. *Phys. Rev. D*, **97**(2018)06, 063525.
- [32] C. Garcia-Garcia, E.V. Linder, P. Ruiz-Lapuente and M. Zumalacarregui. Dark energy from α -attractors: phenomenology and observational constraints. *JCAP*, **08**(2018) 022.
- [33] Y. Akrami, S. Casas, S. Deng, V. Vardanyan. Dark energy from α -attractors: phenomenology and observational constraints. *JCAP*, **04**(2021) 006.
- [34] David H. Lyth and Antonio Riotto. Particle physics models of inflation and the cosmological density perturbation. *Phys. Rept.*, 314:1–146, 1999.
- [35] P.A.R. Ade et. al. BICEP2, Planck Collaboration. Joint Analysis of BICEP2/*KeckArray* and *Planck* Data. *Phys. Rev. Lett*, **114**(2015)101301.